JOURNAL OF MATERIALS SCIENCE 31 (1996) 224–231

A high resolution electron microscopic study of the microstructure in rapidly solidified Al–Li–Cu–Mg–Zr alloys

L. C. ZHANG*, A. Q. HE, H. Q. YE, Y. C. ZHANG‡
Laboratories of Atomic Imaging of Solids and ‡ Microcrystals, Institute of Metal Research, Academia Sinica, Wenhua Road, Shenyang 110015, People's Republic of China

The microstructure in rapidly solidified Al–Li–Cu–Mg–Zr alloys has been reexamined by transmission electron microscopy (TEM). The results show that the weakening intermetallic phases, e.g. hexagonal, Z, face centred cubic (f.c.c), T, and tetragonal, H, (new phase) phases, exist in alloys with relatively high contents of Mg besides the strengthening phases. The sizes of these weakening intermetallic phases are on the scale of micrometres. The newly found tetragonal H phase, having parameters of $a = 2.8$ nm and $c = 2.4$ nm, was observed to coexist with the Z phase, and has a defined orientation relationship with the Z phase. High resolution images reveal that there are planar defects and 90° domains in the Z phase, multiple twins in the T phase, and two well defined crystallographic orientation relationships between the Z and T phases.

1. Introduction

Aluminium–lithium alloys are of considerable interest to the aerospace community due to their high specific strengths and stiffness. Unfortunately, other properties, such as low ductility, low fracture toughness and poor corrosion resistance, have limited their application considerably. The precipitating process of intermetallic phases while some alloying elements, such as Cu, Mg and Zr, are added to Al–Li binary alloys becomes very complicated, and is not clearly understood so far. Precipitation for various intermetallic phases is closely related to the alloy composition, alloy preparation process and heat treatment procedure. According to the literature, in terms of their influence on material properties, all intermetallic phases precipitated in Al–Li system alloys after ageing can roughly be divided into two types: finer strengthening phases, e.g. δ′-Al_3Li, T_1-Al_2CuLi and S′-Al_2CuMg, and coarse weakening phases, e.g. T_2-Al_6Li_3Cu, R-Al_5Li_3Cu, δ-AlLi, Al–Fe and Al–Fe–Cu intermetallic. Former works focus mainly on precipitation and crystal structure characterization of strengthening phases as they affect the mechanical properties of the casting materials; little study has covered these weakening phases, especially their structural defects and their structural links. However, research on weakening phases, especially in crystallographic links, was stimulated due to the discovery of an icosahedral quasicrystal T_2-Al_6Cu_3Li in Al–Li–Cu alloys [1–3]. Recently, some reexamination of Al–Li–Cu–Mg, Al–Li–Zn and Al–Li–Zn–Cu alloys has resulted in the identification of several complicated intermetallic phases in the vicinity of $Al_{0.6}(Cu, Zn)_{0.1}(Li, Mg)_{0.3}$, namely the so-called R, Z, C and τ phases [4, 5]. Moreover, their intimate structural relationships to the T_2 quasicrystal phase also have been considered. In terms of crystallography, these complicated intermetallic phases (including the T-Al_2LiMg phase) and T_2 consist of similar structural units, such as blocks of icosahedra, dodecahedra and tricontehedra, which often makes them intergrow with each other. Shiflet *et al.* [6] and Yang *et al.* [7] interpreted six types of shear planes in the R phase by means of quasilattice vectors introduced for the study of quasicrystals, implying a structural link between R and T_2 phases resulting from the transformation behaviour from T_2 to R phase. Zhou and Shiflet [8] observed a well defined crystallographic orientation relationship between the R and Z phases with the same basic building units in the Al–Li–Cu alloy, and [9] have detected a relation between the Z and T phases. (The Z phase belongs to a hexagonal system, with unit cell parameters of $a = 1.403$ nm, $c \approx 2a$, and a $P6_3/m.m.c.$ space group, and its chemical composition is $Al_{0.59}Li_{0.26}Mg_{0.10}$ [6]. The T phase belongs to an f.c.c. lattice, with parameters of $a = 2.058$ nm, and chemical composition Al_2LiMg, but its space group has not been determined due to the presence of many crystal defects. Audier *et al.* [5] proposed $Fd\bar{3}m$ as its space group, according to the relation between T and C phases).

In this paper, a recent high resolution electron microscopic study of the microstructure in rapidly

* *Present address*: State Key Laboratory of Advanced Metal Materials, University of Science and Technology Beijing, Beijing 100083, People's Republic of China.

0022–2461

solidified Al–Li–Cu–Mg–Zr alloys is presented. As the chemical composition of the alloys studied is multiple element, and the rapid solidification technique is adopted in alloy preparation, a new intermetallic phase was first detected. Experimental results also show that the content of elemental Mg in the alloys affects the kind of precipitates which may influence the mechanical properties of the studied materials. Furthermore, high resolution images reveal a great amount of crystallographic information in the hexagonal Z and f.c.c. T phases.

2. Experimental procedure

The alloys, with compositions (wt %) of Al–3.20 Li–1.16 Cu–4.04 Mg–0.26 Zr and Al–2.28 Li–1.47 Cu–2.03 Mg–0.28 Zr, were prepared by gas atomization, followed by vacuum hot pressing and extrusion. They were numbered as alloys one and two, respectively. After solution heat treatment (510 °C 0.5 h^{-1} for alloy one, and 530 °C 0.5 h^{-1} for alloy two), the specimens were quenched in cold water and then annealed at 120 °C 24 h^{-1} for alloy one and 150 °C 24 h^{-1} for alloy two. The TEM specimens was thinned first by two-jet electropolishing in an electrolyte containing one part HNO_3 and three parts CH_3OH (by volume), then ion milled. High resolution electron microscopic observation was performed in a Jeol 2000EX(II) electron microscope with Cs = 0.8 mm, and with a point resolution of 0.21 nm. Selected area electron diffraction (SAED) patterns and X-ray energy despersive spectrum analysis (EDAX) of intermetallic phases were carried out in Jeol 200CX microscope with double tilts and a Phillips EM 420, respectively.

3. Results and discussion

3.1. The morphologies and properties of the alloys

TEM observations to alloy one after heat treatment show the existence of α-Al solid solutions, δ′ and

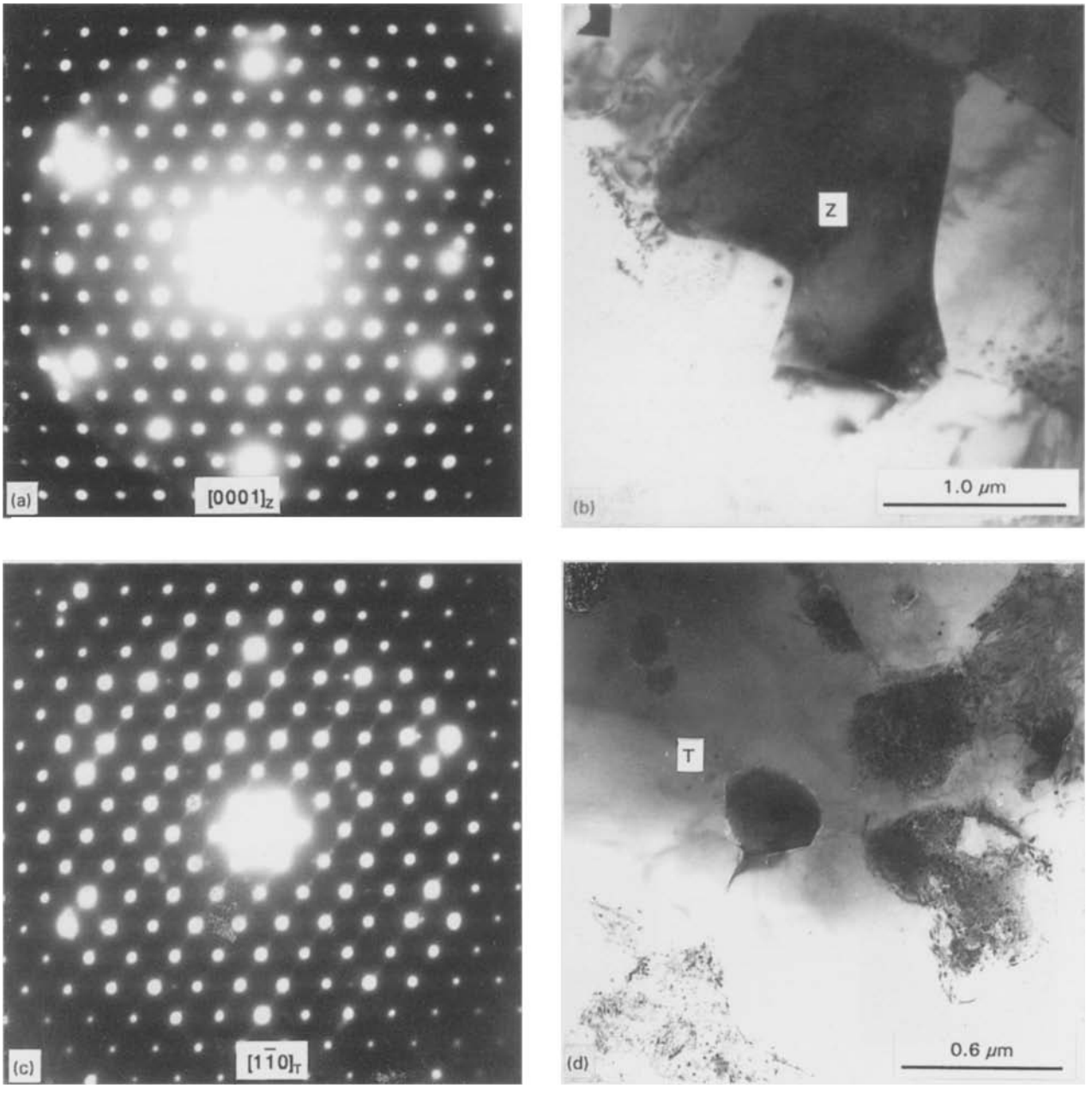

Figure 1 SAED patterns and morphology of (a, b) the hexagonal Z phase, and (c, d) the f.c.c. T phase.

TABLE I The mechanical properties and precipitates in the present study

Alloy No.	σ_b (MPa)	$\sigma_{0.2}$ (MPa)	δ (%)	Phases
Alloy one	524.2	424.5	10	α-Al, δ′, Al–Fe
Alloy two	465.5	371.9	4	α-Al, δ′, Z, T, H

a small amount of Al-Fe intermetallic phase, no other strengthening phases are detected. In alloy two, after similar heat treatment, besides α-Al solution and the strengthening δ′ phase, there exist as large number of Z, T phases and a small amount of H phase (the last is new phase found in the present work, and will be detailed later). The sizes of the Z and T phases are all in a scale of micrometres, generally the Z phase is a little larger than the T phase in size as shown in Fig. 1. Formation of the Z and T phases should be attributed to the relatively high Mg content of elemental Mg in alloy two as this phase contains elemental Mg. Comparison of precipitates with properties between alloys one and two, shown in Table I, suggests that these intermetallic compounds, i.e. the Z, T and H phases, might be principally responsible for the poor mechanical properties of the material studied.

3.2. A new tetragonal phase and its relation with the Z phase

A new tetragonal phase was observed in alloy two, and named the H phase. Fig. 2 shows the sequence of SAED patterns possessing the same electron diffraction spot row, but in different orientations from the H phase, which were taken by rotating different angles (seeing tilting degrees in the figure) around the [0 1 0]* axis starting with the [0 0 1] zone pattern. The absence of electron diffraction spots $(hk0)$ with odd h or k values (in the [0 0 1] zone pattern) should be attributed to systematic forbidden reflection introduced by the inner crystal structure of the H phase; the forbidden reflection introduced by the inner crystal structure of the H phase; the forbidden reflections in the $[1\,0\,\bar{2}]$, $[1\,0\,\bar{1}]$ and $[5\,0\,\bar{2}]$ zone patterns are visible because of double diffraction. The structural detail of the H phase is being studied and will be reported in the future. Fig. 3 is a projection along this tilting axis and it shows the H phase has a tetragonal lattice. The parameters of the H phase can be calculated to be $a = 2.8$ nm and $c = 2.4$ nm $[c/a = 0.866 \approx (3/2)^{1/2}]$ according to these SAED patterns.

Fig. 4 is the electron micrograph showing the coexistence of the H and Z phases. The SAED analysis shows that both of the Z and Z′ regions are all the Z phase, only being differently orientated to the H phase. Fig. 5 is the high resolution image of position "a" in Fig. 4. The areas labelled "Z" and "H" correspond to the Z phase viewing along its $[1\,0\,1\,0]_Z$ direction and the H phase along its $[0\,0\,1]_H$ direction, respectively. From this figure, an orientation relationship between the two phases can be given, i.e. $(1\,0\,0)_H//(\bar{1}\,2\,\bar{1}\,0)_Z$, $[0\,1\,0]_H//[0\,0\,0\,1]_Z$. It is also shown that no obvious phase interface exists between them along this direction. In fact, the $(1\,0\,\bar{1}\,0)$ planar spacing of the Z phase, $d_{(1\,0\,\bar{1}\,0)} = 1.21$ nm, is equal to half a length of the c-axis of the tetragonal H phase, thus it is reasonable that the two phases can be connected rather well along the [1 0 0 1] direction of the H phase (or along the $[1\,0\,\bar{1}\,0]$ direction of the Z phase). Fig. 6a–c shows the SAED patterns of the H, Z and Z′ regions in Fig. 4, the detailed analysis displays that it is two equal orientation relationships that exist between the H and Z regions, the H and Z′ regions,

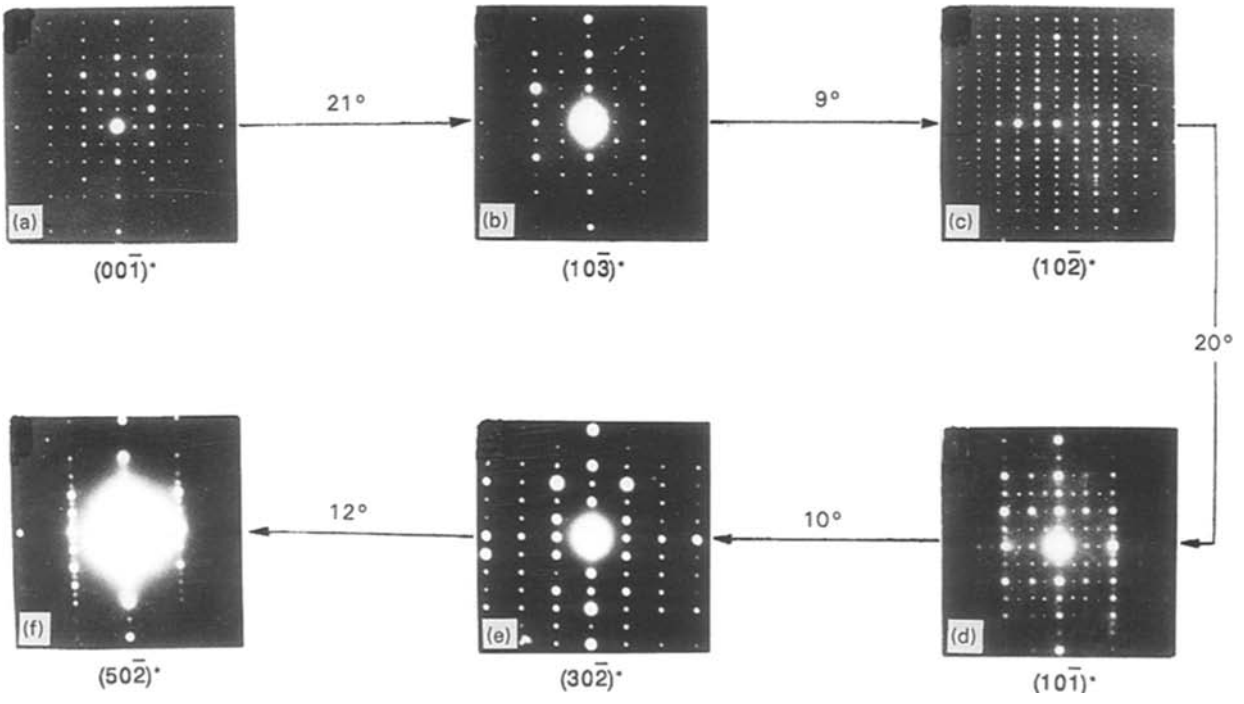

Figure 2 The sequence of SAED patterns from the H phase. The angles among these patterns have been illustrated.

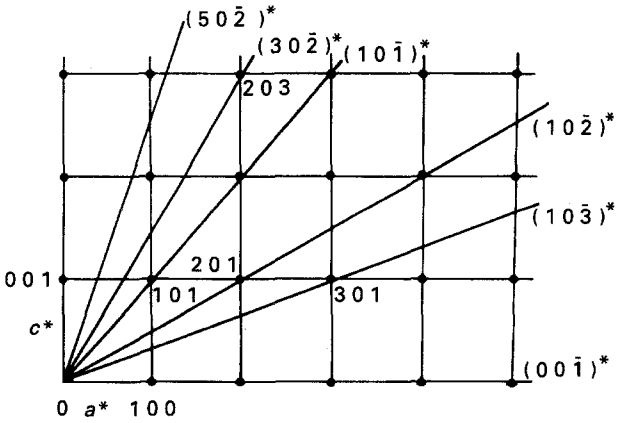

Figure 3 A plot of different $(u0w)^*$ planes (thick lines) projected on $(0\,1\,0)^*$ of the H phase according to the above six SAED patterns and their angles.

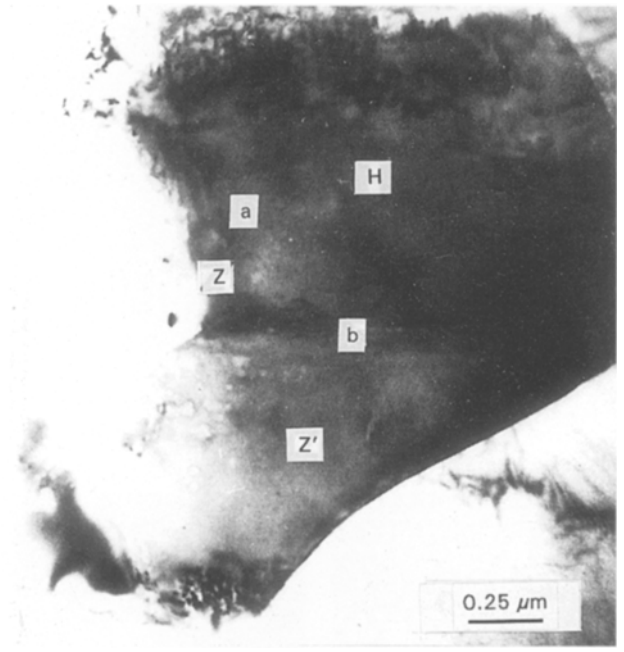

Figure 4 Electron micrograph showing coexistence of the H and Z phases.

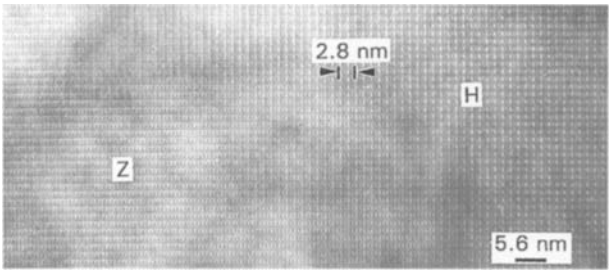

Figure 5 The high resolution image of the position "a" in Fig. 4 displaying the relationship between the H and Z phases: $(1\,0\,0)_H//(\bar{1}\,2\,\bar{1}\,0)_Z$, $[0\,1\,0]_H//[0\,0\,0\,1]_Z$.

being, respectively, given by

$$(1\,0\,0)_H//(\bar{1}\,2\,\bar{1}\,0)_Z,\ [0\,1\,0]_H//[0\,0\,0\,1]_Z$$

and

$$(0\,1\,0)_H//(\bar{1}\,2\,\bar{1}\,0)_Z,\ [1\,0\,0]_H//[0\,0\,0\,1]_Z$$

The orientation illustration is shown in Fig. 7.

Although the H and Z phases, with no obvious boundary, are difficult to distinguish in Fig. 4, and they cannot be revealed separately by dark field imaging because of their densely covered electron diffraction spots caused by their large lattice parameters, the high resolution image clearly shows the difference between the two phases, as shown in Fig. 5. Plenty of experiments on the specimen display that the larger size Z phase appears frequently to coexistence with the H phase in the above two mentioned orientations. Also EDAX analysis of the H and Z phases (results given in Table II) shows that both of the two phases contain the same chemical elements, i.e. Al, Cu, Mg, and have similar contents to one other; the light element Li is undetected. This implies that the H phase may be the metastable phase corresponding to the Z phase.

3.3. Crystal defects in Z phase

Fig. 8 shows high resolution images of several types of planar defects on the $\{1\,\bar{1}\,0\,0\}$, $\{0\,0\,0\,1\}$ planes of the Z phase. Except for these defects, a particular 90° rotational domain exists in the Z phase, which is shown in Fig. 9. The domain boundary is apparently relatively flat in this low magnification image. A high resolution image of the domain in the Z phase is displayed in Fig. 10, where the two blocks labelled "A" and "B" orientate along the $[1\,1\,\bar{2}\,0]_Z$ and $[0\,0\,0\,1]_Z$ directions, respectively, (the bright dots in Fig. 10b should correspond to the position, between tricontehedras, of the main basic building units of the Z phase [5]; and this problem is not important in defining the domain relationship in this paper). This relationship could be described as $[0\,0\,0\,1]_A//[1\,1\,2\,0]_B$, $[1\,\bar{1}\,0\,0]_A//[1\,\bar{1}\,0\,0]_B$, coinciding with the interface on $(1\,1\,0\,0)_A//(1\,1\,0\,0)_B$. In fact, block "A" is linked to "B" by rotating 90° with each other around the $[1\,1\,0\,0]_B$ direction. The absence of any defect structure inside "A" and "B", and coherency at the interface, indicates that the length of the c-axis should be double the length of the a-axis for the hexagonal Z phase.

3.4. Structural relationships between the Z and T phases

Two well defined crystallographic orientation relationships between the Z and T phases have been detected by high resolution image analysis, as shown in Fig. 11. The two blocks labelled "Z" and "T" in Fig. 11a correspond to the Z phase viewing along its $[1\,1\,\bar{2}\,0]_Z$ direction and the T phase along its $[1\,\bar{1}\,0]_T$ direction, respectively. From this figure, an orientation relationship, I, can be established as $[0\,0\,0\,1]_Z//[1\,1\,1]_T$, $[1\,1\,\bar{2}\,0]_Z//[1\,\bar{1}\,0]_T$, and the interface is on the $(0\,0\,0\,1)_Z//(1\,1\,1)_T$, which is consistent with the well known Burger's relationship between hexagonal and cubic phases [10]. In Fig. 11b, high resolution imaging of the two blocks, labelled "Z" and "T", are again along the $[1\,1\,\bar{2}\,0]_Z$ and $[1\,\bar{1}\,0]_T$ directions, respectively; however, they show another orientation relationship, II: $[1\,\bar{1}\,0\,0]_Z//[0\,0\,1]_T$, $[1\,1\,2\,0]_Z//[1\,1\,0]_T$, and the interface is now on the

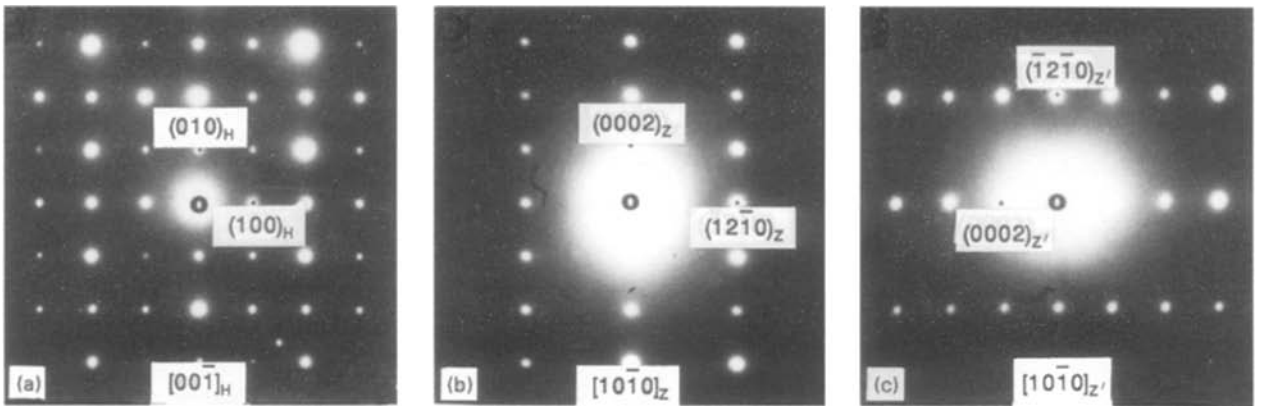

Figure 6 SAED patterns from the (a) H, (b) Z, and (c) Z′ regions of Fig. 4.

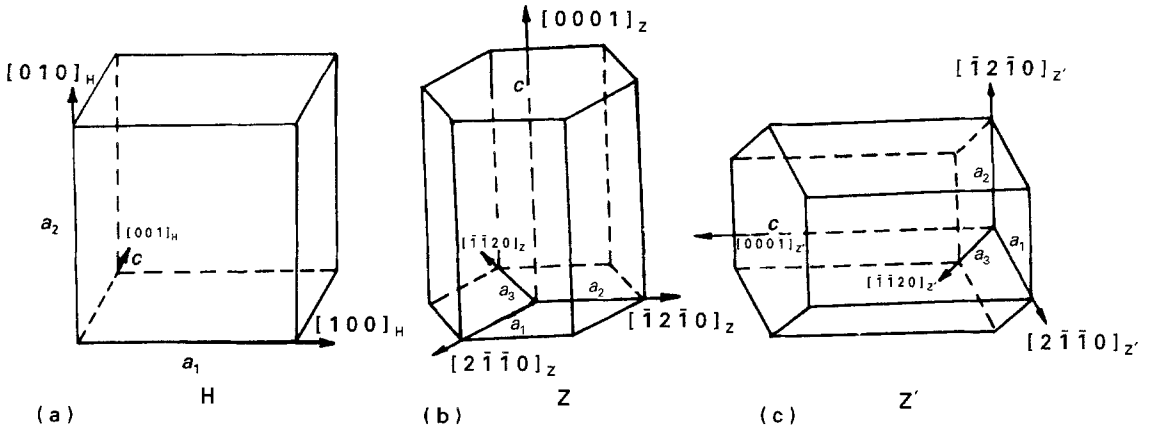

Figure 7 Schematic orientations for the (a) H, (b) Z, and (c) Z′ regions of Fig. 4.

TABLE II The X-ray energy spectrum quantitative analysis to the H and Z phases

Phase (at %)	Al	Mg	Cu
H	74.52	17.59	7.89
Z	73.54	16.04	10.42

$(1\bar{1}00)_Z//(0002)_T$. The frequency of the second type of orientation relationship appears relatively less than that of the first one.

Fig. 12a, b shows the typical morphology of the first and the second Z–T orientation relationship, respectively. The two blocks labelled "A" and "B" in Fig. 12b correspond separately to the Z phase along its $[0001]_Z$ and $[11\bar{2}0]_Z$ directions; both their relation with T phase belong to the second Z–T structural relationship. From the figure, the precipitated phase is very small, generally 10 nm in width (the "Z" blocks in Fig. 12a) so as to reduce the strain energy introduced by the misfit at the phase interface (the misfit is calculated to be about 3.7%); on the other hand the misarrangement appeared in the Z phase near the interface (the position "C" in Fig. 12b) accordingly loosening the interface stress.

In the author's observation, no interfacial dislocations and steps can be detected, while the Z phase is precipitated over several unit cell thicknesses on the habit plane of the T phase, even though this is a relatively high misfit at the phase interface, as shown in Fig. 12a. It shows that the phase interfaces still remain rather coherent due to the similarity and link of the complicated crystal structure in the Z and T phases; and the elastic strain of their similar structural blocks

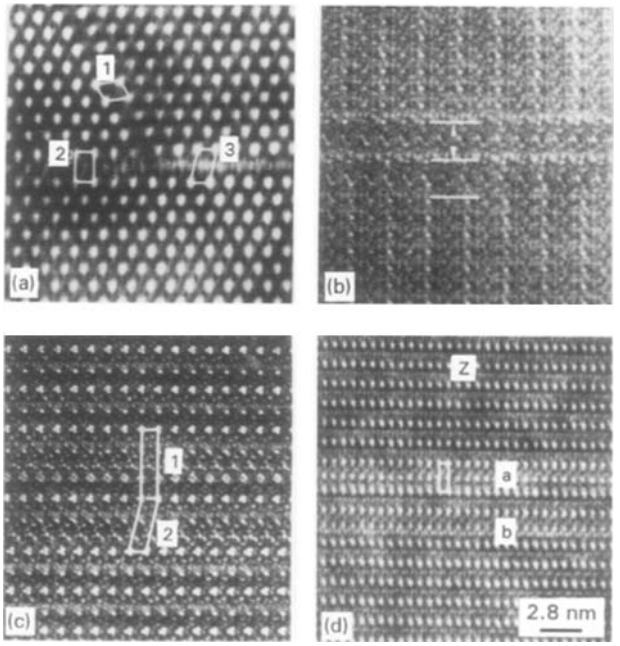

Figure 8 Planar defects on (a) the $\{1\bar{1}00\}$ plane of the Z phase, viewed along the $[0001]_Z$ direction; (b) the $\{1\bar{1}00\}$ plane of the Z phase, viewed along the $[1\bar{1}20]_Z$ direction; (c) the $\{0001\}$ plane of the Z phase, viewed along the $[1\bar{1}20]_Z$ direction; and (d) the $\{0001\}$ plane of the Z phase, viewed along the $[\bar{1}100]_Z$ direction.

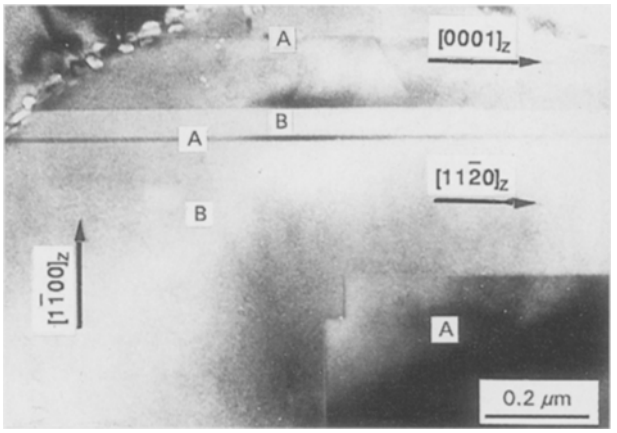

Figure 9 The bright field image of the 90° rotation domain and domain boundary in the Z phase.

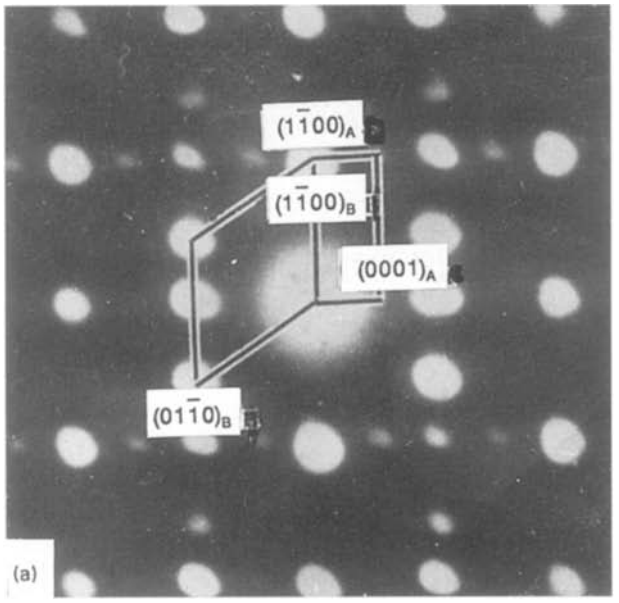

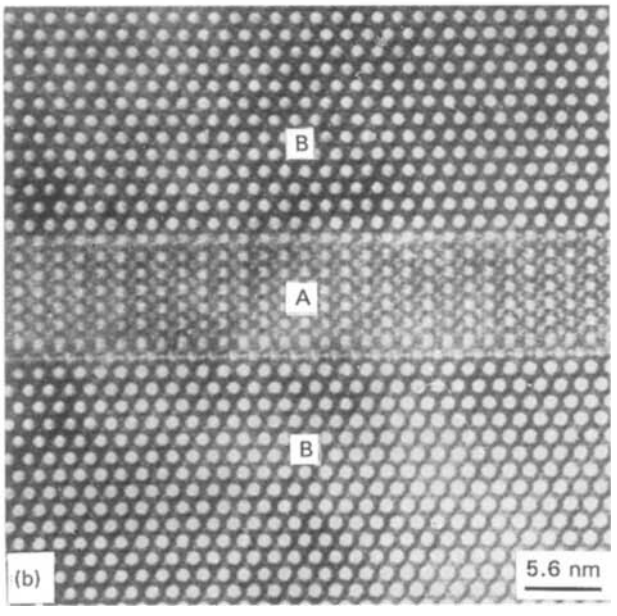

Figure 10 (a) The composite electron diffraction pattern and (b) the corresponding high resolution image of the variants "A" and 'B" viewed along the $[11\bar{2}0]_Z$ and $[0001]_Z$ direction, respectively.

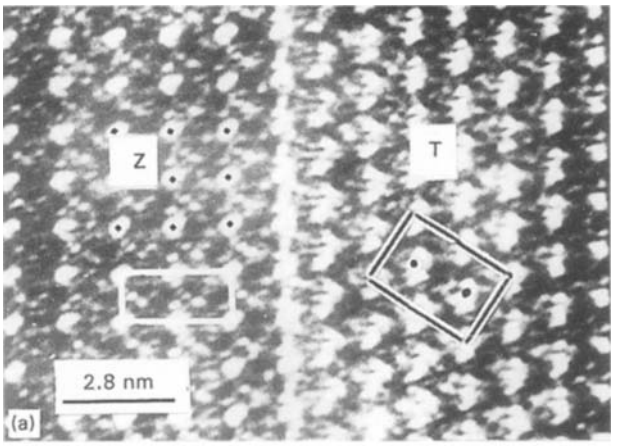

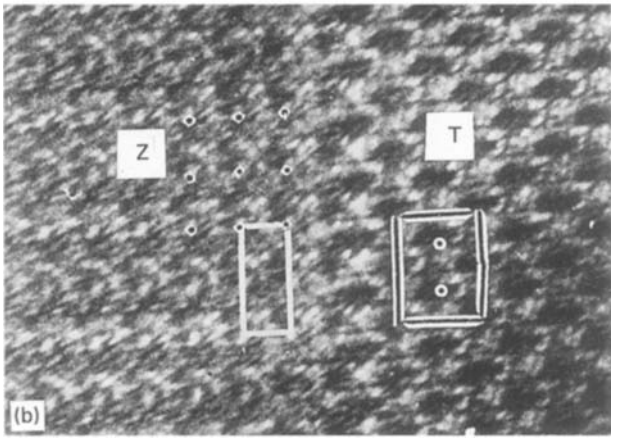

Figure 11 Direct illustrations of orientation relationships between the Z and T phases: (a) the first type, and (b) the second type.

could contain the misfit in the interphase boundary. In fact, the Z and T phases have an intimate structural relation to each other, the main basic building units of the two phases are tricontahedra and dodecahedra respectively, and a tricontrahedra is formed by capping 12 more (Al, Cu) atoms to the 12 pentagonal faces of a dodecahedra [5]. Similar information was recently reported in [11], which pointed out that the $(1\,1\,0)_L/(1\,0\,0)_C$ interface between C14 laves and C phases also still remains very well coherent, although a high lattice misfit (2.56%) exists at the C/L phase interface, because of the similarity of the complex crystal structure in the laves and C phases. Certainly, this containment to the lattice misfit by the elastic strain of their similar structural blocks is within certain limits, and while the Z and T phases of both large sizes coincide, a distortion appears at the end of the relatively small phase interface, as shown in Fig. 12b. As a result, the interface stress between the Z and T phases has a strong restraint to the growth thickness (direction perpendicular to the interface) of these coexisting phases, as identified in Fig. 12a.

Fig. 13a shows a planar defect on the (1 1 1) plane of the T phase, viewed along the $[1\,1\,\bar{2}]_Z$ direction (the direction perpendicular to that in Fig. 11a). The size of such a planar defect is equal to a unit cell of Z phase (projected along $[1\,\bar{1}\,0\,0]_Z$ direction). The two phases obey the first Z–T orientation relationship. Thus, the planar defect could be considered as the Z phase if the

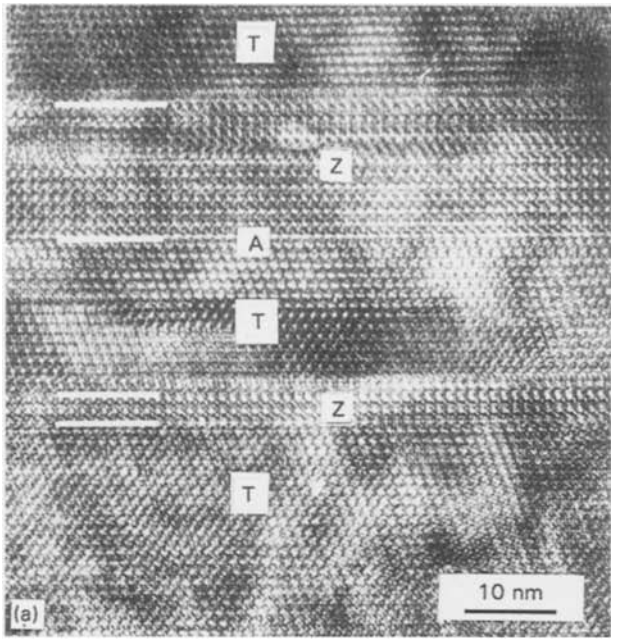

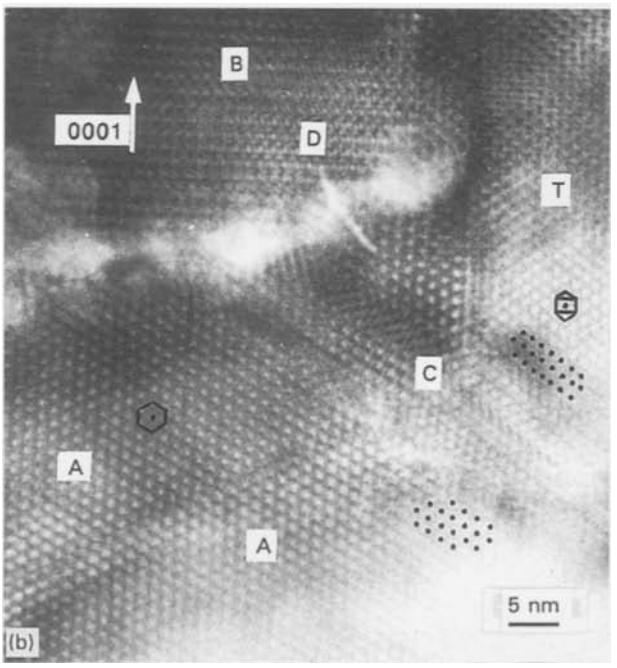

Figure 12 Typical morphology corresponding to (a) the first Z–T relationship, and (b) the second Z–T relationship.

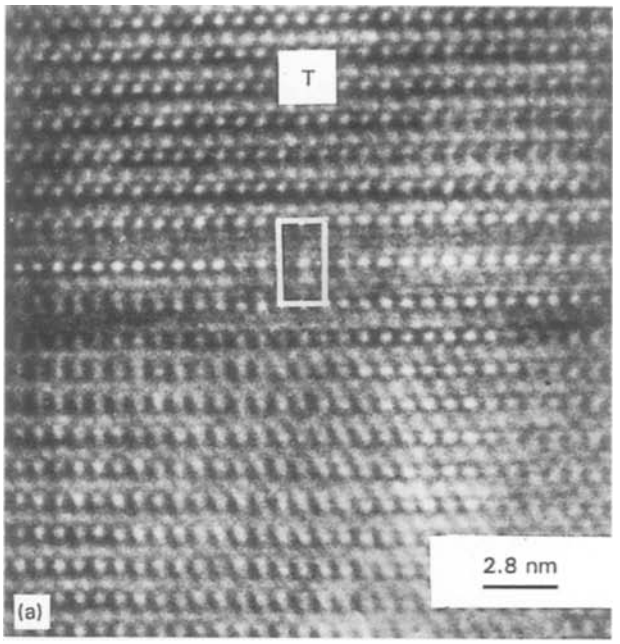

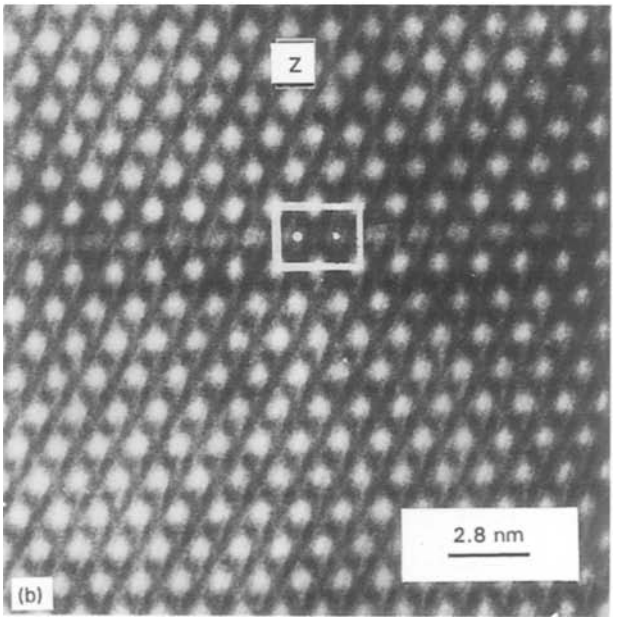

Figure 13 Planar defect on (a) the (1 1 1) plane of the T phase, viewed along the $[1\,1\,\bar{2}]_T$ direction; and (b) the $(1\,\bar{1}\,0\,0)$ plane of the Z phase, viewed along the $[0\,0\,0\,1]_Z$ direction.

planar defect area is extended along the thick direction. Fig. 13b shows another planar defect on the $(1\,\bar{1}\,0\,0)$ plane of the Z phase viewed along the $[0\,0\,0\,1]_Z$ direction, a similar analysis to the defect indicates that it should be a unit cell of the T phase viewed along the $[1\,\bar{1}\,0]_T$ direction, according to the second Z–T orientation relationship.

Fig. 14, taken along the $[1\,\bar{1}\,0]_T$ direction, displays the planar defect structures that occurred mainly on the $\{1\,1\,1\}$ and $\{0\,0\,2\}$ type planes of the f.c.c. T phase, reflecting two types of the Z–T relations. The four-fold twins are marked are to four in order, respectively. The twin boundaries are shown to be very complicated. For example, a rectangular unit can be found the in the boundary between the two and three variants, and its size is equal to half a unit cell of Z phase viewed along the $[1\,1\,\bar{2}\,0]_Z$ direction. The relation between the unit and two, three variants also shows the first type of orientation relationship between the Z and T phases. Another example is a rectangular unit between the 2,2′-variants, with the same size as the above one, but differently orientated to the two variant. This region is large in size and can be regarded as the Z phase domain, the analysis shows that the Z phase with several unit cells in thickness viewed along the $[1\,1\,\bar{2}\,0]_Z$ direction precipitates on the (0 0 2) plane of the T phase, according to the second Z–T orientation relationship.

Based upon the above analysis, one could deduce that successive growth of defects in either of the Z and T phases might produce another phase domain, as a result of their intimate structural link.

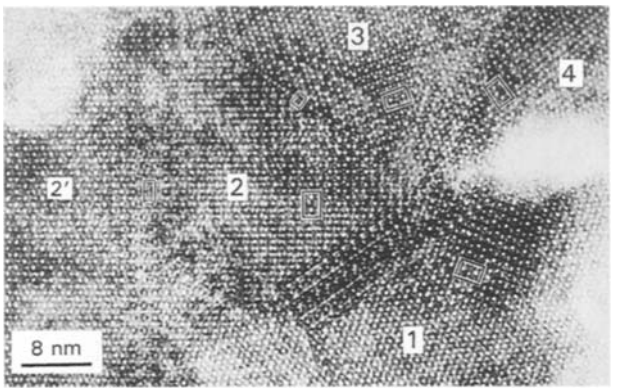

Figure 14 Multiple twin structures and domain boundaries, showing planar defects on the {1 1 1} and {0 0 2} planes of the T phase, which, in fact, could be regarded as the domain structures of the hexagonal Z phase.

4. Conclusions

Through a systematic study of microstructure in the rapidly solidified Al–Li–Cu–Mg–Zr alloys, one can conclude that besides the main strengthening phase, i.e. δ′ phase, a large amount of Z and T phases and a small amount of H phase (Z, T and H phases all contain elemental Mg) are present in the alloy containing relatively high Mg. These intermetallic phases have a scale of micrometres and are considered as weakening phases for the materials. The new found phase, i.e. the H phase, is tetragonal with parameters of $a = 2.8$ nm, $c = 2.4$ nm, and coexists with the Z phase. There is a defined relationship between the H and Z phases: $[0\,0\,1]_H//[\bar{1}\,2\,\bar{1}\,0]_Z$, $[0\,1\,0]_H//[0\,0\,0\,1]_Z$, but no obvious phase interface between them. Furthermore, high resolution images reveal a 90° rotational domain in the hexagonal Z phase (around the $[1\,1\,1\,0]$ direction), and four-fold twins in the f.c.c. T phase. It is also shown that there exists two defined orientation relationships between the Z and T phases: (I), $[0\,0\,0\,1]_Z//[1\,1\,1]_T$, $[1\,1\,\bar{2}\,0]_Z//[1\,\bar{1}\,0]_T$, with the interfacial plane $(0\,0\,0\,1)_Z/(1\,1\,1)_T$, and (II) $[1\,\bar{1}\,0\,0]_Z//[0\,0\,1]_T$, $[0\,0\,0\,1]_Z//[1\,1\,0]_T$, with the interfacial plane $(1\,1\,\bar{1}\,0)_Z/(0\,0\,2)_T$.

References

1. W. A. CASSADA, G. J. SHIFLET and S. J. POON, *Phys. Rev. Lett.* **56** (1986) 2276.
2. B. DUBOST, J. W. LANG, M. TANAKA, P. SAINFORT and M. AUDIER, *Nature* **324** (1986) 48.
3. Y. SHEN, G. J. SHIFLET and S. J. SOON, *Phys. Rev. B* **38** (1988) 5332.
4. A. LOISEAU and G. J. LAPPASSET, *Phil. Mag. Lett.* **56** (1987) 165.
5. M. AUDIER, C. JANOT, M. DER BOISSIEU and B. DUBOST, *ibid.* **60** (1989) 437.
6. G. J. SHIFLET, Q. B. YANG, D. S. ZHOU and S. J. POON, *Phil. Mag. A* **64** (1991) 483.
7. Q. B. YANG, D. S. ZHOU and G. J. SHIFLET, *ibid.* **65** (1992) 1395.
8. D. S. ZHOU and G. J. SHIFLET, *Script Metall. Mater.* **25** (1991) 1999.
9. L. C. ZHANG, A. Q. HE and H. Q. YE, *ibid.* **30** (1994) 63.
10. W. G. BURGER, *Physica* **1** (1934) 561.
11. H. Q. YE, *J. Chinese Electron Microsc. Soc.* **12**(2) (1993) 145.

Received 8 February 1994
and accepted 22 June 1995